

Electric modulation of magnetic anisotropy on the granule/matrix interface of a permalloy/PZT composite

Bo Chen ^{1,*} Dan-Feng Pan,² Mei-Ling Duan,¹ and Pan-Long An¹

¹*Department of Physics, School of Science, North University of China, TaiYuan 030051, China*

²*School of Electronic Science and Engineering, NanJing University, NanJing 210093, China*



(Received 29 April 2019; revised manuscript received 17 August 2019; published 14 October 2019)

In this work, the electric modulation of magnetic anisotropy is investigated on a granule/matrix interface of a Py/PZT composite. Outside the Py/PZT interface, the electric polarization is derived through the Thomas-Fermi model and mean field approximation. Inside the Py/PZT interface, the magnetizing energy is derived through the spin-split model and spherical shell approximation. As the Py volume fraction varies from 0.0% to 0.8%, the electric polarization evolves from radiationlike to vortexlike distribution, while the magnetizing energy evolves from symmetric-type to asymmetric-type distribution. Under downward and upward polarization, parallel and perpendicular magnetization are preferred, respectively. As the granule diameter or matrix thickness is varied, the downward polarization induces unstable parallel magnetic anisotropy, while the upward polarization induces stable perpendicular magnetic anisotropy. This work is beneficial for achieving electrostatic manipulation of a magnetic vortex.

DOI: [10.1103/PhysRevB.100.134418](https://doi.org/10.1103/PhysRevB.100.134418)

I. INTRODUCTION

The permalloy (Py) alloy, whose molecular formula is $\text{Fe}_{20}\text{Ni}_{80}$, has been widely and deeply investigated in spintronics. The Py bulk is ferromagnetic at room temperature. However, due to the competition between demagnetizing energy and exchange energy, the ground magnetic state in the Py nanostructure evolves dramatically with its size. As the Py size is ~ 10 and ~ 100 nm, the ground magnetic state is the “flower” and the “Landau/diamond” type, respectively [1]. The latter is also called the magnetic vortex state, where the in-plane magnetization curls around the core, while the magnetization inside the core rotates out of plane [2–4]. The vortex orientation can be switched by magnetic field or electric current [5–8], which advances information storage and process technology.

The magnetic anisotropy is crucial to achieving magnetic vortex in Py nanostructure. Because the exchange energy is stronger than magnetocrystalline energy, the magnetic anisotropy in Py bulk is nearly zero. However, if grown under particular conditions, the Py nanostructure exhibits a certain perpendicular magnetic anisotropy [9,10]. As a result, the magnetic stripe domain emerges, where the out-of-plane magnetization component is upward and downward periodically [11,12]. In a Py nanodisk, the perpendicular magnetic anisotropy induces transformation between magnetic vortex and bubble state [13]. In a Py nanotube, the perpendicular magnetic anisotropy stabilizes the magnetic vortex state at zero magnetic field [14].

Up to now, the magnetic anisotropy is usually introduced into a Py nanostructure by a particular synthesizing

atmosphere, which is irreversible after being grown. If such magnetic anisotropy could be reversibly and nonvolatily manipulated by an external field, the magnetic vortex in the Py nanostructure would be switched more flexibly. In the author’s previous work, a Ni/PZT composite with a granule/matrix interface was designed, where the component of the top and bottom electrode is Au and SrRuO_3 (SRO), respectively [15]. The converse magnetoelectric coupling is theoretically predicted through the mean field approximation and spherical shell approximation. As the electric polarization is upward and downward, certain perpendicular and parallel magnetic anisotropy is induced, respectively. Both Ni and Py are ferromagnetic metals. Thus similar coupling would be present in a Py/PZT composite.

Currently, the magnetic state in the Py nanostructure is mainly studied through micromagnetic simulation [16]. This method describes the magnetic quantity by a discrete grid with a regular element. For example, to obtain the demagnetizing energy, the magnetization and demagnetizing field must be calculated in each element. As the Py size is increased by n times, the computing complexity will be increased by n^3 times. In contrast to the micromagnetic simulation, the author’s previous work describes a magnetic quantity by continuous space [15]. For example, the demagnetizing field is expressed as a vector varying with spherical coordinates r , θ , and φ . The computing complexity of such analytical method is size independent; i.e., the computing load is permanent no matter how large the size reaches.

In this work, the author develops the previous theory in order to describe the electric polarization and magnetizing energy. On the granule/matrix interface of a Py/PZT composite, the converse magnetoelectric coupling is predicted through the present theory. According to the electric polarization rotation and magnetizing energy evolution, the electric modulation of magnetic anisotropy is proved.

*BoChen@nuc.edu.cn

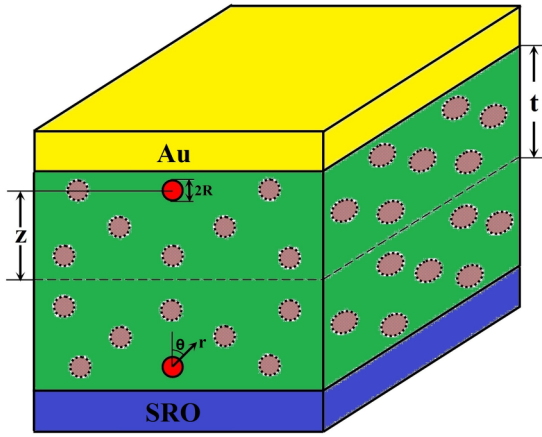


FIG. 1. The illustration for the granule/matrix interface of Py/PZT composite.

II. METHOD

A. Electric polarization

As illustrated by Fig. 1, the Py granule is dispersed in the PZT matrix, while the top and bottom electrodes are constituted by Au and SRO, respectively. The granule diameter and matrix thickness are expressed by $2R$ and $2t$, respectively. Because the SRO substrate prefers the (001)-crystalline structure of PZT matrix, the in-plane strain of the PZT matrix is estimated as $[a_{\text{PZT}} - a_{\text{SRO}}]/a_{\text{PZT}} = -2.2\%$ [17]. As a result, the spontaneous polarization of the PZT matrix is out-of-plane orientated [18]. Accordingly, as the spontaneous polarization is upward and downward, it is expressed by $P_0 \leq 0$ and $P_0 \geq 0$, respectively. Around an isolated Py granule, the electrostatic screening potential is derived through the Thomas-Fermi model combined with the Laplace equation and infinite boundary condition. For interactive Py granules, the electrostatic screening potential is modified through the perturbation method and mean field approximation. Details are seen in the author's previous work [15].

Taking the Gauss law and electrostatic potential continuity on the Py granule surface, the electrostatic charge is deduced. For an isolated and interactive Py granule, the surface density of the electrostatic charge is expressed in Eqs. (1) and (2), respectively:

$$\sigma^{(0)} = \frac{\epsilon_r[(\delta_{\text{Au}} - \delta_{\text{SRO}})t + (\delta_{\text{Au}} + \delta_{\text{SRO}})z]}{[R + \epsilon_r\delta_{\text{Py}}][\epsilon_r(\delta_{\text{Au}} + \delta_{\text{SRO}}) + 2t]} P_0 + \frac{2[\epsilon_r(\delta_{\text{Au}} + \delta_{\text{SRO}}) - t]R}{[R + 2\epsilon_r\delta_{\text{Py}}][\epsilon_r(\delta_{\text{Au}} + \delta_{\text{SRO}}) + 2t]} P_0 \cos \theta, \quad (1)$$

$$\sigma = \sigma^{(0)} + \eta \sum_{n=0}^3 n P_{n,0} \left(\frac{z + R \cos \theta}{t} \right)^{n-1} \cos \theta + \eta \sum_{n=0}^3 (n+1) P_{n,1} L_n(\cos \theta). \quad (2)$$

The η represents the volume fraction of the Py granule in the composite. The electric polarization $P_{n,0}$ and $P_{n,1}$ are functions of P_0 . Note that the unit is identical between electric polarization and surface charge density. The n th-order Legendre

polynomial is labeled by $L_n(\cos \theta)$. The spontaneous polarization $P_0 = 40 \mu\text{C}/\text{cm}^2$; dielectric constant $\epsilon_r = 100$; and electrostatic screening depths $\delta_{\text{Au}} = 0.06 \text{ nm}$, $\delta_{\text{SRO}} = 0.6 \text{ nm}$, $\delta_{\text{Py}} = 0.12 \text{ nm}$ are adopted here [19–21].

Besides spontaneous polarization, the local polarization depends on the electrostatic screening potential Ψ near the Py/PZT interface, as illustrated by Eq. (3):

$$\vec{P} = \vec{P}_0 + \epsilon_r \epsilon_0 (-\vec{\nabla} \Psi). \quad (3)$$

To describe the local polarization P , the spherical coordinate is set up around each Py granule center, where the φ axis is along the vertical direction. Considering the mirror symmetry about the central longitudinal profile, the P vector is zero along the φ axis; i.e., $P_\varphi = 0$. Substituting the electrostatic screening potential into Eq. (3), the P_r and P_θ are derived in Eqs. (4) and (5), respectively:

$$P_r = P_r^{(0)} + \eta \sum_{n=1}^3 n P_{n,0} \left(\frac{z + r \cos \theta}{t} \right)^{n-1} \cos \theta + \eta \sum_{n=0}^3 (n+1) P_{n,1} \left(\frac{R}{r} \right)^{n+2} L_n(\cos \theta), \quad (4)$$

$$P_\theta = P_\theta^{(0)} - \eta \sum_{n=1}^3 n P_{n,0} \left(\frac{z + r \cos \theta}{t} \right)^{n-1} \sin \theta - \eta \sum_{n=0}^3 P_{n,1} \left(\frac{R}{r} \right)^{n+2} \frac{\partial L_n(\cos \theta)}{\partial \theta}. \quad (5)$$

The first item of the right side is further expressed in Eq. (6):

$$\begin{Bmatrix} P_r^{(0)} \\ P_\theta^{(0)} \end{Bmatrix} = P_0^{(0)} \begin{Bmatrix} \cos \theta \\ -\sin \theta \end{Bmatrix} + P_2^{(0)} (R/r)^2 \begin{Bmatrix} 1 \\ 0 \end{Bmatrix} + P_3^{(0)} (R/r)^3 \begin{Bmatrix} 2 \cos \theta \\ \sin \theta \end{Bmatrix}. \quad (6)$$

Here the electric polarization $P_0^{(0)}, P_2^{(0)}, P_3^{(0)}$ are functions of P_0 .

B. Magnetizing energy

Due to the interaction between Coulomb energy and exchange energy, the electrostatic screening charge on the Py surface is spin split. Taking the spin-dependent potential and dielectric response function, such spin-splitting rate has been derived by other work [21]. Thus, the magnetization of the Py granule is expressed in Eq. (7):

$$M = M_0 - \frac{N^\downarrow - N^\uparrow}{N^\downarrow + N^\uparrow + 4JN^\downarrow N^\uparrow} \mu_B \frac{\sigma}{e\delta_{\text{Py}}}. \quad (7)$$

The spontaneous magnetization $M_0 = 8.59 \times 10^5 \text{ A/m}$, spin-up Fermi density $N^\uparrow = 0.25 \text{ eV}^{-1} \text{ nm}^{-3}$, spin-down Fermi density $N^\downarrow = 1.1 \text{ eV}^{-1} \text{ nm}^{-3}$, and exchange energy constant $J = 0.27 \text{ eV nm}^3$ are adopted here [21]. In the spherical coordinate around each Py granule center, the Py/PZT interface is axially symmetric about the φ axis. Thus the magnetizing angle is defined by $\theta = \theta_m$ and $\varphi = 0$.

In the Py granule, the surface and volume magnetic pole are induced by the magnetization orientation and decay,

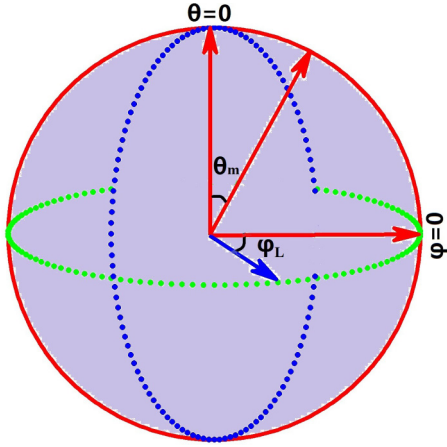


FIG. 2. The illustration for the longitudinal profile in the Py granule. The normal angle of the longitudinal profile is expressed as ψ_L .

respectively. According to the author's previous work, the magnetic pole density is derived through spherical shell approximation [15]. Thus the demagnetizing field in the Py granule is expressed by Eq. (8):

$$\vec{H} = -\frac{\vec{M}_0}{3} + \sum_{n=1}^4 \vec{H}_n^{(s)} + \sum_{n=0}^4 \vec{H}_n^{(v)}. \quad (8)$$

The second and third items are further expressed in Eqs. (9) and (10), respectively:

$$\begin{aligned} \vec{H}_n^{(s)} = & -\vec{\nabla} \left[\frac{r^n}{(2n+1)R^{n-1}} L_n(\cos \theta) \right] H_{n,0} \cos \theta_m \\ & - \vec{\nabla} \left[\frac{r^n}{(2n+1)R^{n-1}} L_n^1(\cos \theta) \cos \varphi \right] H_{n,1} \sin \theta_m, \quad (9) \end{aligned}$$

$$\sum_{n=0}^4 \begin{bmatrix} H_{r,n}^{(v)} \\ H_{\theta,n}^{(v)} \\ H_{\varphi,n}^{(v)} \end{bmatrix} = \begin{bmatrix} H_{r,0}^{(v)} \\ 0 \\ 0 \end{bmatrix} + \sum_{n=1}^4 \begin{bmatrix} g_{r,n} & 0 & 0 \\ 0 & g_{\theta,n} & 0 \\ 0 & 0 & g_{\varphi,n} \end{bmatrix} \begin{bmatrix} H_{r,n}^{(s)} \\ H_{\theta,n}^{(s)} \\ H_{\varphi,n}^{(s)} \end{bmatrix}. \quad (10)$$

The magnetic fields $H_{n,0}$ and $H_{n,1}$ are functions of magnetic pole density. In the author's previous work, the g factor is deduced through spherical shell approximation [15].

At each position in the Py granule, the M vector is expressed by Eq. (11):

$$\begin{bmatrix} M_r \\ M_\theta \\ M_\varphi \end{bmatrix} = M \begin{bmatrix} \sin \theta \cos \varphi \sin \theta_m + \cos \theta \cos \theta_m \\ \cos \theta \cos \varphi \sin \theta_m - \sin \theta \cos \theta_m \\ -\sin \varphi \sin \theta_m \end{bmatrix}, \quad (11)$$

Ultimately, the magnetizing energy density is expressed by Eq. (12):

$$f = -\frac{\mu_0}{2} (H_r M_r + H_\theta M_\theta + H_\varphi M_\varphi). \quad (12)$$

The magnetizing energy F is defined as the integral of $f dV$ throughout the spherical granule. As the magnetization is perpendicular, i.e., $\theta_m = 0$, the axial symmetry about the φ axis is retained. Thus, on any longitudinal profile shown in Fig. 2, the

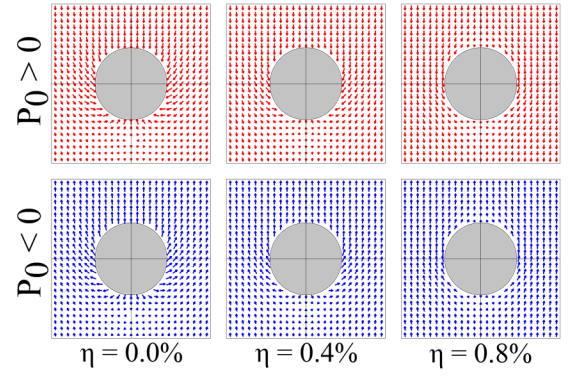


FIG. 3. The distribution of local polarization P in the PZT matrix. The position is $z = 0$. The size is $R = 5.0$ nm and $t = 50.0$ nm.

distribution of f is identical. However, as the magnetization is parallel, i.e., $\theta_m = \pi/2$, the above axial symmetry is broken. Correspondingly, on each longitudinal profile, the distribution of f varies with normal angle ψ_L , as shown in Fig. 2.

III. RESULTS AND DISCUSSION

A. Correlative pattern

Near the Py/PZT interface, the distribution of local polarization P is plotted in Fig. 3. Here the position is $z = 0$, while the size is $R = 5.0$ nm and $t = 50.0$ nm. Far away from the Py/PZT interface, the local polarization P gradually orients toward the spontaneous polarization P_0 ; i.e., P tends to be along the vertical axis. However, on the top and bottom regions of the PZT matrix, the P amplitudes are different from each other, which reflects that the electrostatic screening potential is a nonlinear function of position [15]. Adjacent to the Py/PZT interface, the local polarization P deviates greatly from the spontaneous polarization P_0 . A similar phenomenon has been observed in other works [22,23]. Such deviation evolves with volume fraction η . As $\eta = 0.0\%$ and 0.8% , the deviation is radiationlike and vortexlike, respectively; i.e., the local polarization P is nearly perpendicular and parallel with the Py/PZT interface, respectively. This evolution originates from the electrostatic interaction between several Py granules, which modifies the electrostatic screening potential in the PZT matrix [15].

Because the axial symmetry is broken under parallel magnetization, the distribution of magnetizing energy density f on the longitudinal profile for $\psi_L = \pi/2$ and $\psi_L = 0$ is plotted in Figs. 4 and 5, respectively. Here the position is $z = 0$, while the size is $R = 5.0$ nm and $t = 50.0$ nm. To refine the distribution near the Py granule surface, both the x and y displacements are multiplied by the factor $\exp[(r-R)/(5\delta_{Py})]$. For $\psi_L = \pi/2$ and $\psi_L = 0$, the distribution is ellipselike and circlelike, respectively. Near the Py granule surface, the energy gradient is focused; i.e., the f amplitude is increased or decreased dramatically. A similar phenomenon has been observed in other works [24,25]. Because the axial symmetry is broken, the f amplitude for $\psi_L = \pi/2$ is much higher than that for $\psi_L = 0$. As η is increased from 0.0% to 0.8% , the f amplitude is decreased monotonously, while the f distribution along the x axis transforms from symmetric type to

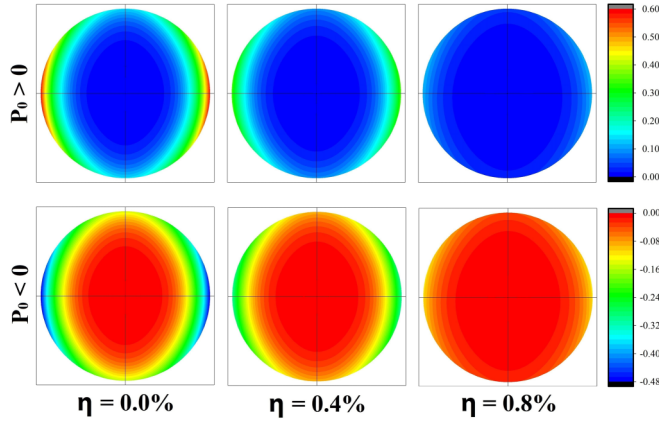


FIG. 4. Under parallel magnetization, the distribution of magnetizing energy density f on the longitudinal profile for $\psi_L = \pi/2$. The position is $z = 0$. The size is $R = 5.0$ nm and $t = 50.0$ nm.

asymmetric type. Such evolution of energy density f is correlative with that of local polarization P ; i.e., the radiationlike and vortexlike P distributions are accompanied by symmetric-type and asymmetric-type f distribution, respectively.

Because the axial symmetry is retained under perpendicular magnetization, the distribution of magnetizing energy density f on any longitudinal profile is plotted in Fig. 6. Here the position is $z = 0$, while the size is $R = 5.0$ nm and $t = 50.0$ nm. Both the x and y displacements are multiplied by the factor $\exp[(r-R)/(5\delta_{Py})]$. The ellipselike distribution is kept on the longitudinal profile for any ψ_L . Under perpendicular and parallel magnetization, the energy gradient is focused on the vertical and horizontal edge, respectively, while the f amplitudes are comparable with each other. Details are seen in Figs. 4 and 6. As η is increased from 0.0% to 0.8%, the evolution of f under perpendicular magnetization is similar to that under parallel magnetization. Such similar evolution originates from the electrostatic interaction between several Py granules, which determines the magnetic pole in the Py granule [15].

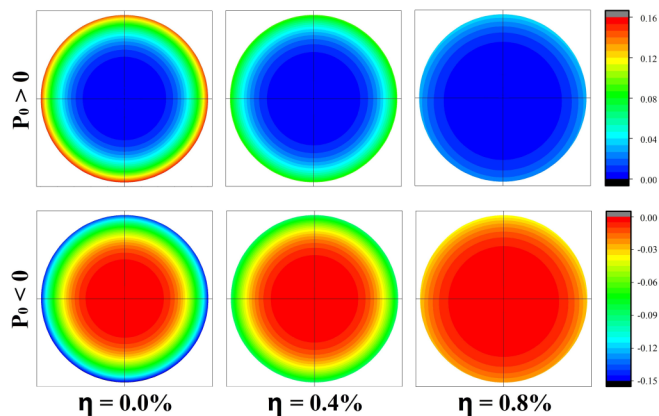


FIG. 5. Under parallel magnetization, the distribution of magnetizing energy density f on the longitudinal profile for $\psi_L = 0$. The position is $z = 0$. The size is $R = 5.0$ nm and $t = 50.0$ nm.

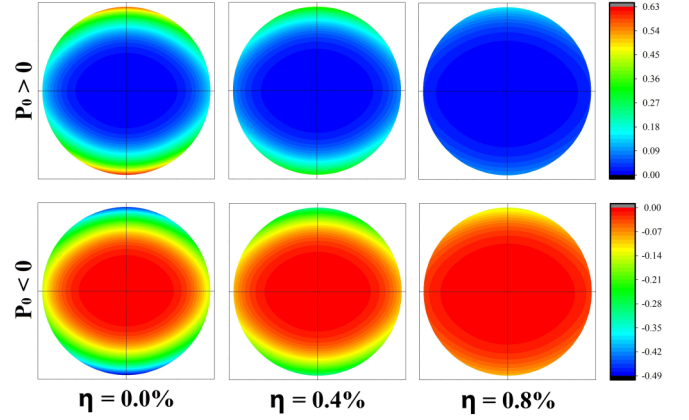


FIG. 6. Under perpendicular magnetization, the distribution of magnetizing energy density f on any longitudinal profile. The position is $z = 0$. The size is $R = 5.0$ nm and $t = 50.0$ nm.

B. Correlative behavior

For $R = 5.0$ nm and $t = 50.0$ nm, the $\bar{\sigma}/P_0$ varying with both z and η is plotted in Fig. 7. By integrating $\sigma \times (dS/S)$ throughout the granule surface, the $\bar{\sigma}$ is deduced in Eq. (13):

$$\bar{\sigma} = \frac{\varepsilon_r(\delta_{Au} - \delta_{SRO})t + \varepsilon_r(\delta_{Au} + \delta_{SRO})z}{[R + \varepsilon_r\delta_{Py}][\varepsilon_r(\delta_{Au} + \delta_{SRO}) + 2t]}P_0 + \eta \frac{2R}{3t}P_{2,0} + \eta \frac{2zR}{t^2}P_{3,0} + \eta P_{0,1}. \quad (13)$$

As spontaneous polarization is downward and upward, i.e., $P_0 > 0$ and $P_0 < 0$, the equivalent charge density $\bar{\sigma}$ on the Py granule surface is generally negative and positive, respectively. As z varies from -45 nm to $+45$ nm, the $\bar{\sigma}$ amplitude is generally decreased, which reflects the electrostatic screening potential is an asymmetric function of position [15]. As η is increased from 0.0% to 0.8%, the $\bar{\sigma}$ amplitude is also decreased gradually. Such evolution originates from the electrostatic interaction between several Py granules, which introduces anharmonic distribution of the electrostatic charge on the granule surface. Details are seen in the author's previous work [15]. Furthermore, the electrostatic charge on the

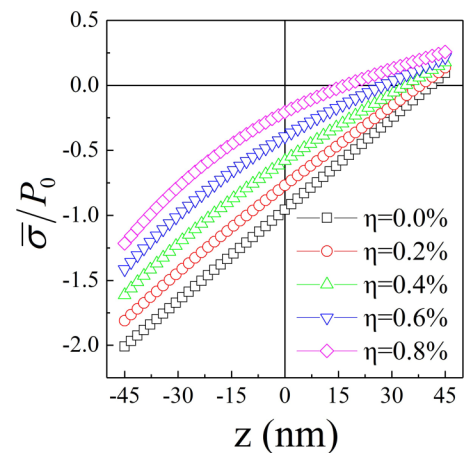


FIG. 7. For $R = 5.0$ nm and $t = 50.0$ nm, the $\bar{\sigma}/P_0$ varying with both z and η .

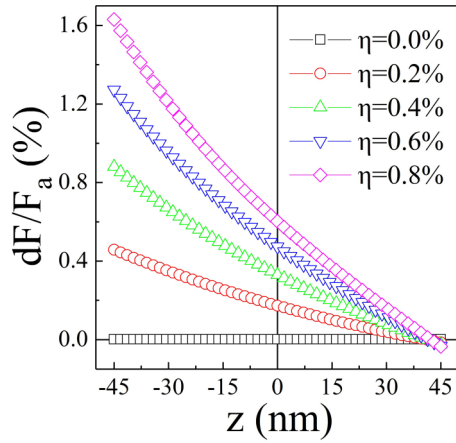


FIG. 8. For $R = 5.0$ nm and $t = 50.0$ nm, the dF/F_a varying with both z and η under downward P_0 .

Py granule surface compensates the electrostatic screening potential in the PZT matrix. Consequently, the leakage current in the Py/PZT composite could stay at a low level.

By integrating $f \times dV$ throughout the granule body, the magnetizing energy F is deduced in Eq. (14):

$$F = F_s(P_0)\sin^2\theta_m + F_c(P_0)\cos^2\theta_m. \quad (14)$$

The characteristic energies F_s and F_c are functions of P_0 . Under perpendicular and parallel magnetization, i.e., $\theta_m = 0$ and $\pi/2$, F reaches the extreme value. Thus, the magnetic anisotropy energy dF is defined as $F_c(P_0) - F_s(P_0)$, which demonstrates the energy difference between perpendicular and parallel magnetization. Under downward and upward P_0 , dF/F_a varying with both z and η is plotted in Figs. 8 and 9, respectively. The size is $R = 5.0$ nm and $t = 50.0$ nm. Here $F_a/V = 8.0 \times 10^2$ J/m³ represents the anisotropy energy density in Py film achieved by other work [11]. As P_0 is downward and upward, i.e., $P_0 > 0$ and $P_0 < 0$, the energy dF stays positive and negative, respectively, which means the parallel and perpendicular magnetizations are the ground state, respectively. Thus, downward and upward P_0 prefers parallel and perpendicular magnetization, respectively. In other words,

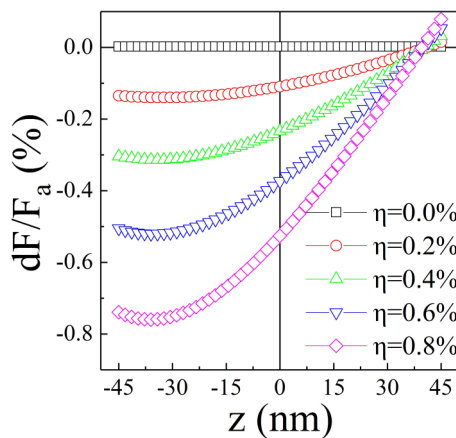


FIG. 9. For $R = 5.0$ nm and $t = 50.0$ nm, the dF/F_a varying with both z and η under upward P_0 .

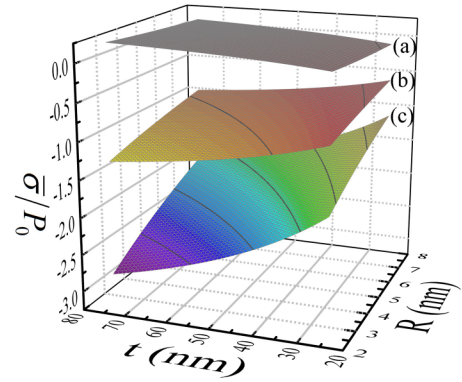


FIG. 10. The $\bar{\sigma}/P_0$ depending on R and t at $\eta = 0.0\%$. The subgraphs (a)–(c) are plotted for $z/(t-R) = +1, 0, -1$, respectively.

certain electric modulation of magnetic anisotropy is realized here.

As position z varies from -45 nm to $+45$ nm, the dF amplitude under downward P_0 is monotonously decreased, while the dF amplitude under upward P_0 reaches the extreme near $z = -45$ nm. Between downward and upward P_0 , such different dF - z evolution originates from the interference of volume and surface magnetizing energy. That is to say, under the upward and downward P_0 , the volume and surface magnetizing energies weaken and strengthen with each other, respectively. Details are seen in the author's previous work [15]. More importantly, under both downward and upward P_0 , the dF amplitude is gradually increased with η . Such dF - η evolution originates from the electrostatic interaction between several Py granules, which introduces the anharmonic distribution of the magnetic moment in the Py granule. Details are seen in the author's previous work [15]. On the whole, as the volume fraction η is increased, the above electric modulation of magnetic anisotropy is enhanced.

C. Size dependence

The equivalent charge density $\bar{\sigma}$ depends on both R and t size. Such dependence for $z/(t-R) = +1, 0, -1$ is plotted in Figs. 10(a)–10(c), respectively. Here the η is fixed at 0.0%. As z varies from $-(t-R)$ to $+(t-R)$, the $\bar{\sigma}/P_0$ generally evolves from negative to zero value. Such evolution is in accordance with that in Fig. 7. As either R varies from 2.5 to 7.5 nm, or t varies from 75 to 25 nm, the absolute $\bar{\sigma}/P_0$ is gradually decreased. However, the $\bar{\sigma}/P_0$ stays negative, generally. Thus, irrespective of the R and t size, the downward and upward polarization P_0 induces negative and positive charge density $\bar{\sigma}$ on the Py granule surface, respectively.

The magnetic anisotropy energy dF also depends on both R and t size. Under downward and upward P_0 , such dependence is plotted in Figs. 11 and 12, respectively. The subgraphs (a)–(c) are plotted for $z/(t-R) = +1, 0, -1$, respectively. Here the η is fixed at 0.8%. As z varies from $-(t-R)$ to $+(t-R)$, under downward and upward P_0 , the dF/F_a generally evolves from positive and negative to zero value, respectively. Such evolution is in accordance with that in Figs. 8 and 9. Thus, as P_0 is downward and upward in the PZT matrix, the parallel

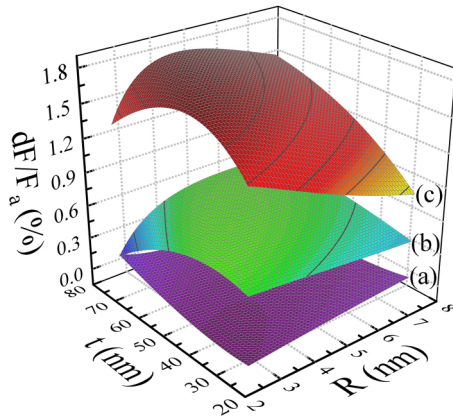


FIG. 11. Under downward P_0 , the dF/Fa depending on R and t at $\eta = 0.8\%$. The subgraphs (a)–(c) are plotted for $z/(t-R) = +1, 0, -1$, respectively.

and perpendicular magnetization is the ground state in the Py granule, respectively.

Under downward P_0 , the absolute dF/Fa reaches the extreme as R varies from 2.5 to 7.5 nm, while it is monotonously decreased as t varies from 75 to 25 nm. Under upward P_0 , the absolute dF/Fa tends to be constant, as either R varies from 2.5 to 7.5 nm, or t varies from 75 to 25 nm. Correspondingly, under downward and upward P_0 , the above parallel and perpendicular magnetic anisotropies are unstable and stable, respectively. In the Py nanostructure, the magnetic vortex state is strongly influenced by perpendicular magnetic anisotropy [13,14]. Thus, the electrostatic manipulation of the magnetic vortex state may be achieved on the granule/matrix interface of the Py/PZT composite.

In the above analysis, the granule diameter stays much smaller than the matrix thickness; i.e., $R \ll t$. However, $R \approx t$ is also possible in the present composite. Considering the electrostatic screening depth is ~ 0.1 nm, as the PZT matrix is polarized, the electrostatic charge only occurs on the Py granule surface. On the other hand, the magnetizing energy

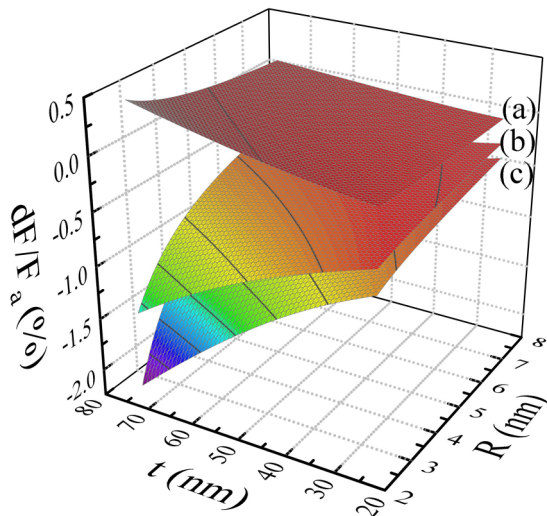


FIG. 12. Under upward P_0 , the dF/Fa depending on R and t at $\eta = 0.8\%$. The subgraphs (a)–(c) are plotted for $z/(t-R) = +1, 0, -1$, respectively.

is determined by the magnetization and demagnetizing field in the whole Py granule volume. Comparing with $R \ll t$, $R \approx t$ implies smaller surface/volume ratio and the weaker electric modulation of magnetic anisotropy. Thus, $R \approx t$ is not considered in the present Py/PZT composite. Furthermore, during fabrication of the actual granule/matrix interface, $R \approx t$ is usually avoided to decrease the leakage current.

IV. CONCLUSION

In this work, the Py/PZT composite with a granule/matrix interface is designed, where the top and bottom electrodes are constituted by Au and SRO, respectively. Outside the isolated Py/PZT interface, the electric polarization is derived through the Thomas-Fermi model. For interactive Py/PZT interfaces, the electric polarization is modified through the perturbation method and mean field approximation. As η varies from 0.0% to 0.8%, the electric polarization evolves from radiationlike to vortexlike distribution. Furthermore, under downward and upward P_0 , the electrostatic charge densities on the Py granule surface are generally negative and positive, respectively.

Inside the Py/PZT interface, the magnetizing energy is derived through the spin-split model and spherical shell approximation. As η varies from 0.0% to 0.8%, the magnetizing energy evolves from symmetric-type to asymmetric-type distribution. Under perpendicular and parallel magnetization, the magnetizing energy gradient is focused on the vertical and horizontal edges of the granule, respectively. Furthermore, under downward and upward P_0 , the magnetizing energy dF stays positive and negative, respectively, implying the parallel and perpendicular magnetization is ground state, respectively.

To perform the size dependence, R is varied from 2.5 to 7.5 nm, while t is varied from 75 to 25 nm. First, the absolute $\bar{\sigma}/P_0$ is gradually decreased, while the $\bar{\sigma}/P_0$ stays negative, generally. Second, under downward P_0 , the absolute dF/Fa reaches the extreme with R , while it is decreased with t . Third, under upward P_0 , the absolute dF/Fa tends to be irrespective of both R and t . Thus, the downward polarization induces unstable parallel magnetic anisotropy, while the upward polarization induces stable perpendicular magnetic anisotropy. This work is beneficial for achieving electrostatic manipulation of the magnetic vortex.

Besides the electrostatic screening, the electrostrictive strain may occur in the PZT matrix, which is usually characterized by a butterflylike curve [26]. Near the coercive and saturated states, the electrostrictive strain reached the positive and negative maximum, respectively. Under the remanent state, the electrostrictive strain tends to zero. In this work, no external voltage is applied between the top and bottom electrodes; i.e., the PZT matrix is under the remanent state. Further considering the clamping of the substrate, the present electric modulation of magnetic anisotropy is hardly influenced by electrostrictive strain.

ACKNOWLEDGMENTS

This work is supported by the Science Foundation of North University of China (Grant No. 2017026), and the Applied Basic Research Foundation of Shanxi Province (Grant No. 201801D221143).

- [1] S. Hankemeier, R. Frömter, N. Mikuszeit, D. Stickler, H. Stillrich, S. Putter, E. Y. Vedmedenko, and H. P. Oepen, *Phys. Rev. Lett.* **103**, 147204 (2009).
- [2] C. F. Adolff, M. Hanze, A. Vogel, M. Weigand, M. Martens, and G. Meier, *Phys. Rev. B* **88**, 224425 (2013).
- [3] S. A. Puig, N. D. Valle, C. Navau, and A. Sanchez, *Appl. Phys. Lett.* **104**, 012407 (2014).
- [4] W. Yu, P. S. Keatley, P. Gangmei, M. K. Marcham, T. H. J. Loughran, R. J. Hicken, S. A. Cavill, G. van der Laan, J. R. Childress, and J. A. Katine, *Phys. Rev. B* **91**, 174425 (2015).
- [5] S. Erokhin and D. Berkov, *Phys. Rev. B* **89**, 144421 (2014).
- [6] S. Rößler, S. Hankemeier, B. Krüger, F. Balhorn, R. Frömter, and H. P. Oepen, *Phys. Rev. B* **89**, 174426 (2014).
- [7] M. Noske, A. Gangwar, H. Stoll, M. Kammerer, M. Sproll, G. Dieterle, M. Weigand, M. Fahnle, G. Woltersdorf, C. H. Back, and G. Schutz, *Phys. Rev. B* **90**, 104415 (2014).
- [8] M. Urbanek, V. Uhlir, C. H. Lambert, J. J. Kan, N. Eibagi, M. Vanatka, L. Flajsman, R. Kalousek, M. Y. Im, P. Fischer, T. Sikola, and E. E. Fullerton, *Phys. Rev. B* **91**, 094415 (2015).
- [9] S. Finizio, S. Wintz, D. Bracher, E. Kirk, A. S. Semisalova, J. Förster, K. Zeissler, T. Weßels, M. Weigand, K. Lenz, A. Kleibert, and J. Raabe, *Phys. Rev. B* **98**, 104415 (2018).
- [10] D. R. Cao, L. N. Pan, X. H. Chen, Z. K. Wang, H. M. Feng, Z. T. Zhu, J. Xu, Q. Li, S. D. Li, J. B. Wang, and Q. F. Liu, *J. Phys. D: Appl. Phys.* **51**, 025001 (2018).
- [11] S. Voltan, C. Cirillo, H. J. Snijders, K. Lahabi, A. García-Santiago, J. M. Hernández, C. Attanasio, and J. Aarts, *Phys. Rev. B* **94**, 094406 (2016).
- [12] S. Singh, H. Gao, and U. Hartmann, *Phys. Rev. B* **98**, 060414(R) (2018).
- [13] C. Moutafis, S. Komineas, C. A. F. Vaz, J. A. C. Bland, and P. Eames, *Phys. Rev. B* **74**, 214406 (2006).
- [14] M. Zimmermann, T. N. G. Meier, F. Dimberger, A. Kákay, M. Decker, S. Wintz, S. Finizio, E. Josten, J. Raabe, M. Kronseder, D. Bougeard, J. Lindner, and C. H. Back, *Nano Lett.* **18**, 2828 (2018).
- [15] B. Chen, N. N. Su, W. L. Cui, and S. N. Yan, *Phys. Lett. A* **382**, 1124 (2018).
- [16] M. Noske, H. Stoll, M. Fahnle, R. Hertel, and G. Schutz, *Phys. Rev. B* **91**, 014414 (2015).
- [17] K. Liang, P. Zhou, Z. J. Ma, Y. J. Qi, Z. H. Mei, and T. J. Zhang, *Phys. Lett. A* **381**, 1504 (2017).
- [18] P. E. Janolin, N. A. Pertsev, D. Sichuga, and L. Bellaiche, *Phys. Rev. B* **85**, 140401(R) (2012).
- [19] M. Y. Zhuravlev, R. F. Sabirianov, S. S. Jaswal, and E. Y. Tsymlal, *Phys. Rev. Lett.* **94**, 246802 (2005).
- [20] V. G. Kukhar, N. A. Pertsev, H. Kohlstedt, and R. Waser, *Phys. Rev. B* **73**, 214103 (2006).
- [21] V. Gunawan and R. L. Stamps, *Phys. Rev. B* **85**, 104411 (2012).
- [22] X. B. Tian, X. H. Yang, P. Wang, and D. Peng, *Appl. Phys. Lett.* **103**, 242905 (2013).
- [23] J. J. P. Peters, G. Apachitei, R. Beanland, M. Alexe, and A. M. Sanchez, *Nat. Commun.* **7**, 13484 (2016).
- [24] F. C. Medeiros Filho, L. L. Oliveira, S. S. Pedrosa, G. O. G. Rebouças, A. S. Carrico, and A. L. Dantas, *Phys. Rev. B* **92**, 064422 (2015).
- [25] L. L. Oliveira, A. L. Dantas, S. S. Pedrosa, G. O. G. Rebouças, R. B. da Silva, J. M. de Araújo, and A. S. Carriço, *Phys. Rev. B* **97**, 134413 (2018).
- [26] T. X. Nan, Z. Y. Zhou, J. Luo, M. Liu, X. Yang, Y. Gao, S. Rand, and N. X. Su, *Appl. Phys. Lett.* **100**, 132409 (2012).